An Equivalent Circuit Model with Variable Effective Capacity for $LiFePO_4$ Batteries

Cecilio Blanco, Luciano Sanchez, *Member, IEEE*, Manuela Gonzalez, Juan C. Anton, *Member, IEEE*, Victor Garcia, Juan C. Viera.

***Abstract*—A new approach to equivalent circuit models for LiFePO4 batteries is presented in this paper. The proposed battery model is a semi-physical nonlinear dynamic model with variable effective capacity. Fuzzy logic has been used to capture the nonlinear behavior of the battery in combination with continuous time differential equations. Fuzzy logic blocks are embedded in a state-space dynamic model as nonlinear constructive blocks. The proposed model has been validated for three different LiFePO4 batteries. The model provides an intuitive physical analogy between charging LiFePO4 batteries and filling a semi-rigid tank, useful for explanatory purposes.**

***Index Terms*—$LiFePO_4$ batteries, Effective capacity, modeling**

I. Introduction

A high specific energy density makes Li-ion batteries the best option for electric vehicles (EV) and hybrid electric vehicles (HEV), in particular the LiFePO4 battery due to its intrinsic safety, low toxicity, high cycle-lifetime, high power capability, reliability, large availability of materials, low cost and flat voltage profile. The main drawbacks of this technology are its relatively low energy density, poor lithium diffusion and poor electronic conductivity [1], [2]. However, several approaches are being pursued to overcome the first two issues, such as the use of nanostructured materials in its chemistry composition and carbon coating [3].

Battery management systems (BMS) are used in EV and HEV applications to ensure the optimal use of batteries. Some key tasks of BMS are to control the charge process and determine the State of Charge (SOC), State of Health (SOH) and remaining runtime of the battery. The SOC, SOH and remaining runtime cannot be directly measured; they have to be inferred from model algorithms. This is not an easy task due to the nonlinear behavior of batteries. Thus, the correct performance of BMS depends on the use of battery models that can describe battery dynamics [4]-[8].

The following effects in battery behavior can be observed when charge/discharge cycles are carried out at different rates: a) Major changes in the battery slope when the battery is near the empty or full states; b) Less charge can be stored in the battery when the charge current is increased; c) Less charge can be drawn from the battery when the discharge current is increased, although the remaining charge will be available after a resting period; d) Hysteresis of the charge/discharge process; and e) Changes in battery voltage during resting periods, when no current flows through the battery

A wide variety of models have been developed to reproduce battery behavior. They may be classified as first principle models, equivalent circuit models and black-box models. First principle models [9]-[12] are based on a description of the electrochemical, thermodynamic and transport phenomena that take place in the battery. They consist of partial differential equations and ordinary differential equations and are suitable for understanding electrochemical reactions in the battery. Although they are likely to be the most accurate and most reliable models, they depend on constructive parameters not provided by battery manufacturers. These models are best suited for optimizing the physical aspects of electrodes and electrolyte. Black box models [13]-[16] have no physical meaning, being based on measured data and statistical approaches. However, there are concerns regarding their capability for extrapolating to cases not provided in the training data. They are suitable when very complex models are difficult to solve using existing modeling methods. Equivalent circuit models (ECM) [17]-[29] are situated midway between first principle models and black box models. They use electrical circuit elements to describe battery behavior. ECM are based on a theoretical background, but are simpler than first principle models and do not depend on constructive parameters.

A new ECM is proposed in this paper which reproduces all the aforementioned effects of battery behavior in addition to enabling determination of the stored charge. The model combines non-linear black boxes with equations describing battery behavior. Although this methodology was first described in [30], it has not been previously applied to battery modeling. These black boxes, inserted in the differential equations as constructive blocks, are fuzzy rule-based systems (FRBS).

The paper is organized as follows. The model is presented in

 This work was supported in part by the Regional Ministry of the Principality of Asturias and Spanish Ministry of Science and Innovation (MICINN) under Grants SV-PA-13-ECOEMP-63 and TIN2011-24302, respectively.

Cecilio Blanco, Manuela Gonzalez, Juan C. Anton and Juan C. Viera are with the Department of Electrical and Electronic Engineering, University of Oviedo, 33208 Gijon, SPAIN. (e-mail: cecilio@uniovi.es, mgonzalez@uniovi.es, anton@uniovi.es, viera@uniovi.es)

Luciano Sanchez is with the Department of Computers, University of Oviedo, 33208 Gijon, SPAIN. (e-mail: luciano@uniovi.es)

Victor Garcia is with the Department of of Physical and Analytical Chemistry, University of Oviedo, 33208 Gijon, SPAIN. (e-mail: victorg@uniovi.es)

Section II and a physical analogy is used to explain how it works. The mathematical formulation is developed in Section III. Section IV describes the testing procedure and the experimental setup, while the experimental results are presented and discussed in Section V. Finally, Section VI presents the conclusions of the paper.

II. Model Operation

Different types of ECM are used for Li-ion batteries. According to [17], most ECM fall into three basic categories: runtime-, impedance- and Thevenin-based models.

Runtime-based models are used to simulate de runtime of a battery. These models use a complex circuit network to simulate battery runtime and DC voltage response for a constant discharge current. Inaccuracy increases as the load current varies [18], [19]. These models are mainly used in SPICE-compatible simulators.

Impedance-based models are derived using an electrochemical impedance spectroscopy (EIS) measurement to obtain the AC response of a cell over a broad range of frequencies [20]-[22]. These models consist of a voltage source, which varies with the SOC, and a complex circuit network of resistors, capacitors, inductors, constant-phase-elements and Warburg impedances. This network can then be related to the behavior of the battery observed via EIS measurements. EIS is still a laboratory technique that cannot be easily used in embedded systems, so this kind of model is not suitable for real time applications.

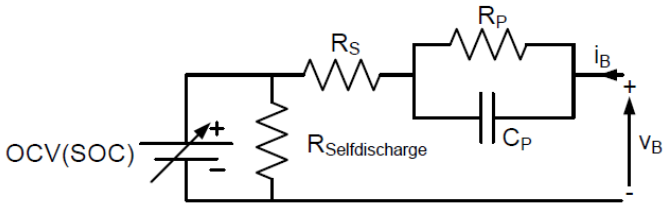

Fig. 1. Thevenin equivalent circuit model.

Thevenin-based models are good at capturing transients, but cannot predict battery runtime [23]-[26]. In their basic form, they consist of a SOC-dependent voltage source, a series resistor and an RC parallel network: see Fig. 1. The parallel capacitance, CP, and the parallel resistance, RP, are used to characterize the transient response of the battery resulting from diffusion and charge transfer, as well as effects related to the electric double layer capacitance at the interface between the electrolyte and the active materials. The series resistance, RS, represents the ohmic impedance on the contacts, electrodes, electrolyte and separator. The source voltage is the open circuit voltage (OCV) of the battery at equilibrium, which depends on the SOC and temperature. The OCV quantitatively represents the SOC. $R_{Selfdischarge}$ is used to model the self-discharge process in the battery, although it is not represented or used in most cases. This kind of ECM is the most widely applied to LiFePO4 batteries [23]-[26].

The combination of these ECM, in particular the Thevenin and run-time models, can exploit the positive attributes of each [17], [27]-[29]. However, none of these types of ECM is able to reproduce the changes in the open circuit voltage of the battery when a current is not circulating through it. A new model, which takes into account this effect, is proposed in this paper: see Fig. 2. The series resistance, R_1, represents the ohmic impedance of the battery and is used to characterize the charge/discharge losses in the battery. The capacitor, C_{eff}, represents the effective capacity of the battery. The stored charge in this capacitor is the stored charge in the battery. Small capacities (double layer capacity) are not relevant on the time scale of the model. Resistance R_2 is used to model the self-discharge process of the battery during long rest periods.

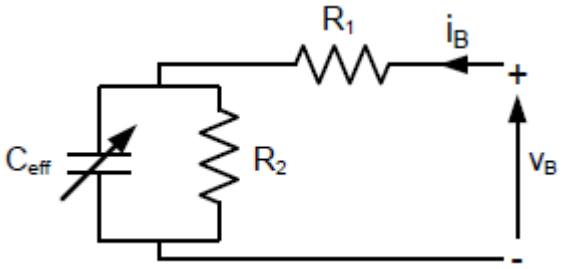

Fig. 2. Proposed equivalent circuit model.

A physical analogy is used to provide a better understanding of how the model works. Think of the battery as the water tank in Fig. 3. The main input/output flow rate to/from the water tank is related to the charge/discharge current, the height of water in the tank is the battery voltage, the volume of water in the tank is the stored charge in the battery and the area of the base of the tank is the effective capacity of the battery, i.e., the quotient between the stored charge and the battery voltage. A drainpipe is used to represent ohmic losses. Water is assumed to flow through the drainpipe only when the battery is being charged or discharged. Drainpipe flow is zero during rest periods.

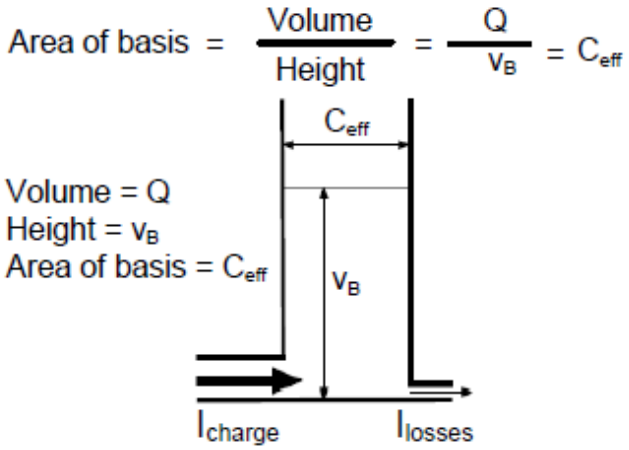

Fig. 3. Physical analogy with constant effective capacity.

When studying the behavior of this physical analogy, it can be seen that battery behavior is not well reproduced: a) If the input/output flow rate is constant, the height of water increases/decreases at the same rate, regardless of whether the tank is almost empty, half full or almost full. The voltage

slope of the battery will hence be constant. b) The total volume of water that can be stored in/extracted from the tank is always the same, regardless of the input/output flow rate. That is, charge stored in/extracted from the battery is always the same, irrespective of the value of the charge/discharge current. c) If the tank is being filled or emptied, the height of water is the same for the same volume of water inside the tank, regardless of whether the tank is being filled or emptied. Thus, the model cannot reproduce the battery voltage hysteresis that takes place when the battery is charged and discharged. d) Once the primary flow rate is zero, the height of water does not vary, i.e., the battery voltage does not vary during rest periods.

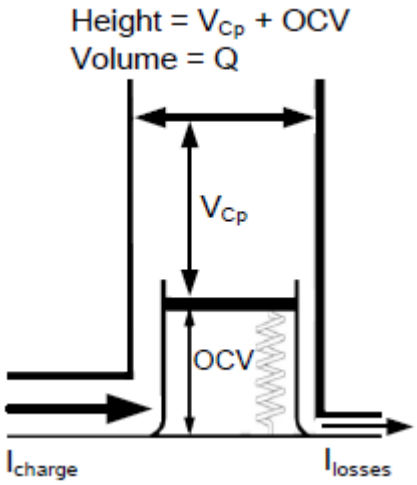

Fig. 4. Physical analogy with constant effective capacity and variable OCV, equivalent to the electrical circuit in Figure 1

This physical analogy, which explains how the model works, cannot reproduce battery behavior because the area of the base of the tank is constant, i.e., the effective capacity of the model, C_{eff}, is considered constant.

In order to reproduce these features of battery behavior, the equivalent circuit in Fig. 1 introduces the voltage source, OCV, which depends on the charge. This amounts to introducing a piston that changes the height of water, as depicted in Fig. 4, partly solving effects (a), (b) and (c), but not (d).

In the proposed equivalent circuit model, the voltage source is removed and a variable effective capacity, C_{eff}, is added. C_{eff} will be modeled as a function of the stored charge, Q, as well as of the sign of the battery current.

Returning to the physical analogy, this needs to be modified to incorporate a variable effective capacity. A semi-rigid tank with the shape shown in Fig. 5 is now assumed. Let us see how the model now reproduces the battery behavior.

The top and bottom of the tank have been tapered. The height of water, which represents the battery voltage, will increase faster when the tank is almost full or almost empty, while the variation in water height is slower in the central part of the tank. Thus, changes in the battery voltage slope are reproduced when the battery is almost full or almost empty. The effective capacity is smaller in these cases.

As the tank is now semi-rigid, it is able to expand when being filled. This means that the effective capacity varies when the battery is being charged. The tank is wider when full. However, the expansion of the tank is not instantaneous, as the expansion rate is lower than the filling rate, unless the filling rate is extremely low. The height of water increases slowly if the input flow rate is low and increases faster if the input flow rate is high. The tank expands as it is filled; when the input flow rate is low, the tank has more time to expand before the water reaches the maximum permissible height. More water can be stored in the tank when it is filled at a low flow rate than when it is filled at a high flow rate. The higher the filling rate, the smaller the effective capacity. Thus, the electric charge that can be stored in the battery is now a function of the charge current.

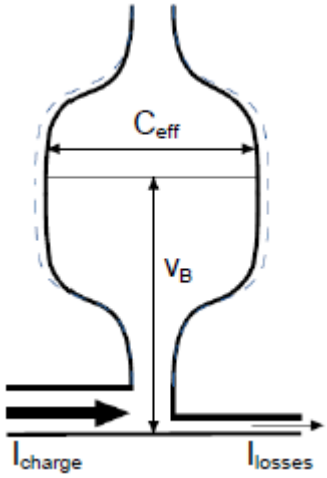

Fig. 5. Physical analogy with variable effective capacity.

As already mentioned, the expansion rate of the tank is lower than the filling rate, so the tank continues to expand after the input flow stops. If the tank continues expanding once the input flow stops, as the volume of water remains constant, the height of water will decrease. That is, the battery voltage now decreases during the rest period following a charging period.

The voltage hysteresis during the charge/discharge cycles, as well as other nonlinearities depending on the sign of the battery current, are modeled by means of different laws of expansion and contraction of the tank during the filling and emptying processes. These laws are included in the model via a function, $\rho(Q, sign(i_B))$, which depends on the stored charge in the battery, Q, and the sign of the battery current $sign(i_B)$. The function $\rho(Q, sign(i_B))$ will be approximated by a FRBS.

III. Model Formulation

The dynamics of the tank can be reproduced by means of the equivalent circuit in Fig. 2, provided that the capacity, C_{eff}, depends nonlinearly on its stored charge. A standard set of nonlinear state-space differential equations will be used to model this behavior:

$$\dot{x}(t) = f(x(t),u(t)) \quad (1)$$
$$y(t) = g(x(t),u(t)) \quad (2)$$

where x(t) is a vector of the state variables, y(t) is a vector of the outputs, and u(t) are the inputs. In this problem, the state variables are the capacity, C_{eff}, and the capacitor voltage, v_{Ceff} The output variable is the battery voltage, v_B, and the input is the charging current, i_B. Therefore:

$$(\dot{C}_{eff},\dot{v}_{Ceff}) = f((C_{eff},v_{Ceff}),i_B) \quad (3)$$
$$v_B = g((C_{eff},v_{Ceff}),i_B) \quad (4)$$

Dividing the vector state equation (3) in two parts and solving (4), the system equations are:

$$\dot{C}_{eff} = f_1(C_{eff},v_{Ceff},i_B) \quad (5)$$
$$\dot{v}_{Ceff} = f_2(C_{eff},v_{Ceff},i_B) \quad (6)$$
$$v_B = i_B \cdot R_1 + v_{Ceff} \quad (7)$$

It is proposed that the nonlinear dependence between the capacity, C_{eff}, and the capacitor charge, $Q = C_{eff} \cdot v_{Ceff}$, possesses a noticeable inertia, which is expressed by means of the first-order system:

$$\dot{v}_{Ceff} = -\frac{v_{Ceff}}{\tau} + \frac{\rho(Q,sign(i_B))}{\tau} \quad (8)$$

where τ is the exponential decay constant and the term

$$\frac{\rho(Q,sign(i_B))}{\tau} \quad (9)$$

is the forcing function. The intuitive meaning of this last equation is that, for small charging currents, in the long term the voltage of the capacitor, v_{Ceff}, is a function, ρ,of its charge Q: i.e., ρ is the shape of the tank. The same occurs for small discharge currents, although the shape of the tank is assumed to be different. Lastly, the decay constant, τ, measures how fast the capacity can change in the absence of a charging current, i.e., how rigid the tank is.

From another perspective,

$$i_B - \frac{v_{Ceff}}{R_2} = \dot{Q} = C_{eff} \cdot \dot{v}_{Ceff} + v_{Ceff} \cdot \dot{C}_{eff} \quad (10)$$

thus

$$\dot{v}_{Ceff} = \left(i_B - \frac{v_{Ceff}}{R_2}\right) \cdot \frac{1}{C_{eff}} - \frac{v_{Ceff}}{C_{eff}} \cdot \dot{C}_{eff} \quad (11)$$

and, solving the system defined by (8) and (11):

$$\dot{C}_{eff} = \left(\frac{1}{\tau} - \frac{\rho(Q,sign(i_B))}{\tau \cdot v_{Ceff}}\right) \cdot C_{eff} + \frac{1}{v_{Ceff}} \cdot \left(i_B - \frac{v_{Ceff}}{R_2}\right) \quad (12)$$

Thus, the proposed system equations (5), (6) and (7) become:

$$\dot{C}_{eff} = \left(\frac{1}{\tau} - \frac{\rho(Q,sign(i_{B}))}{\tau \cdot v_{Ceff}}\right) \cdot C_{eff} + \frac{1}{v_{Ceff}} \cdot \left(i_B - \frac{v_{Ceff}}{R_2}\right) \quad (13)$$

$$\dot{v}_{Ceff} = -\frac{v_{Ceff}}{\tau} + \frac{\rho(Q,sign(i_B))}{\tau} \quad (14)$$

$$v_B = i_B \cdot R_1 + v_{Ceff} \quad (15)$$

These equations depend on the following unknowns:

- The ohmic values of resistors R_1 and R_2
- The nonlinear function $\rho(Q,sign(i_B))$
- The decay constant τ

The numerical values of these parameters can be estimated from experimental data using computational intelligence techniques. As already stated, FRBS are used to approximate the function $\rho(Q,sign(i_B))$. The numerical values of R_1, R_2 and τ, along with the fuzzy rules defining ρ, are numerically optimized to minimize the deviation between the predictions of the model and the available data [31].

IV. Testing Procedures

All tests were carried out at an ambient temperature of 23ºC. Testing-machine adjustments were performed to improve the reliability and accuracy of the measurements. The LFP cells were subjected to the battery testing procedures shown in Fig. 6. The first stage was commissioning, during which the battery was identified and weighed, and the OCV was measured.

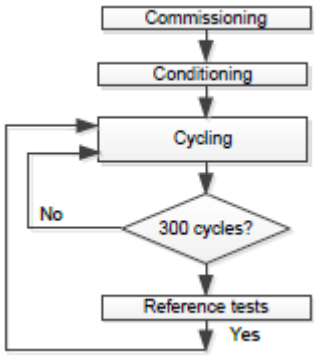

Fig. 6. Flow diagram of the testing procedure.

The conditioning stage began after commissioning. The conditioning test sequence was performed according to the USABC [32]. It consisted of three different constant current discharge cycles. The standard charging method provided by the manufacturer was used to charge the cell. This consists of a constant current (CC) stage at C until the cell reaches the charging cut-off voltage, followed by a constant voltage (CV) stage until the current decreases to 0.05 C. After the capacity had stabilized, a full charge/discharge cycle was performed at a rate of C/25. The results of the C/25 measurements provide a

practical capacity reference with minimal kinetic effects which is close to the maximum capacity attainable by the cell [33].

Once the conditioning of the cell was completed the cycling procedure commenced. Cycling consisted of a series of continuous full charge and discharge cycles at different rates. The cell charging method consisted of a CC stage at 0.3 C until the cell reached the charging cut-off voltage followed by a CV stage until the current decreased to 0.05 C. Stressful or mixed cycling is possible. The battery was subjected to discharges at C/3, C/2 and C. Discharging was carried out at CC until reaching the discharging cut-off voltage recommended by the manufacturer. There was an inactivity period of more than one hour after each charge or discharge until the temperature of the battery fell below 26ºC.

Reference tests were performed every 300 cycles. This test sequence included two standard charges at C with CC discharges at C and C/3, and a final CC charge and discharge at C/25. This set of reference tests was used to characterize the degradation that occurs during the life of the subject test unit and to measure the cell's maximum achievable capacity

V. Computational Intelligent techniques

The numerical experiments justifying the selection of numerical algorithms and other numerical computational aspects are detailed in [34].

A. Fuzzy Systems

0-th order TSK rules were used, in which the antecedent is an AND-combination of statements and the consequent is a real number. The inference procedure is chosen so that the output of the FRBS is functionally equivalent to a spline network [35]. Rules have the following form:

If Q is LOW and i_B is positive then, p = 2.91

where all linguistic terms are triangular fuzzy sets and form strong fuzzy partitions [36]. Three terms were used to describe the current ("POSITIVE", "ZERO" and "NEGATIVE"), while six terms were used to describe the state of charge ("FULL DISCHARGE", "VERY LOW CHARGE", "LOW CHARGE", "MEDIUM CHARGE", "HIGH CHARGE", and "FULL CHARGE").

B. Distal Learning

Standard methods for learning fuzzy rules from data cannot be applied in this context because there are no input-output pairs of the function ρ, although this function is embedded in the differential equations defining the model. The proposed learning is similar to that known as distal learning in neural networks, in which the feedback of the error is obtained after recursive simulations of the model [37].

The first stage in the proposed learning of embedded FRBSs consists in discretizing the differential equations. A discrete-time system is obtained that can be solved in order to obtain $C_{eff}(t)$ and $v_{Ceff}(t)$ given the values of the unknowns at time t-Δt. As the sampling period in this study (5 seconds) is short in relation to the speed of the system, Euler's implicit method [38] is thus sufficient.

Given the input $i_B(t_0+i\Delta t)$, i = 0…N, the initial values $C_{eff}(t0)$ and $v_{Ceff}(t_0)$, the values of R_1, R_2, τ and the function p, recursive estimations of $C_{eff}(t_0+i\Delta t)$ and $v_{Ceff}(t_0+i\Delta t)$ are obtained. Therefore, given a sequence of size N of measurements of battery voltages $\{v^{true}(t_0+\Delta t)\}_{i=1}^{N}$, learning this model requires determining the following 18 unknown parameters:

- R_1, R_2 and τ
- The consequents $c_1, \ldots, c_{15}$ of the rules defining ρ

The best set of parameters is obtained by finding the minimum of the following error function:

$$E(C_{eff}(t_0), v_{Ceff}(t_0), R_1, R_2, \tau, c_1, \ldots, c_{15}) = \sum_{i=1}^{N} (v_B(t_0+\Delta t) - v^{true}(t_0+\Delta t))^2 \quad (16)$$

C. Metaheuristics for optimization

The function E is multimodal, continuous and non differentiable. In addition to this, the parameters must fulfill the following constraints:

a) $R_1 > 0$, $R_2 > 0$, $\tau > 0$

b) $c_1 \le c_2 \le \ldots \le c_{15}$

An extension of Simulated Annealing hybridized with a direct search was applied to find the best set of parameters. This algorithm is based on reference [39] in which this search was shown to be faster than other metaheuristics.

VI. Experimental Results

Three $LiFePO_4$ batteries from different manufacturers, whose characteristics are shown in Table 1, were tested and used to check the proposed model.

TABLE I
TESTED BATTERIES

Manufacturer	MAN#1	MAN#2	MAN#3
Capacity [Ah]	100	100	16
Maximum I charge	3C	3C	5C
Nominal Voltage [V]	3.2	3.2	3.2
Charging cut-off voltage [V]	3.65	3.6	3.65
Discharging cut-off voltage [V]	2.5	2.5	2
Cell geometry	Prismatic	Prismatic	Cylindrical
Dimensions [mm]x[mm]x[mm]	46x182x277	142x67x217,5	40Ø x159,9
Weight[kg]	3.3	3.1	0.5

Cycling test data was used for the identification and validation processes. The sampling frequency was 0.2 Hz. Table 2 shows the charge and discharge currents during cycling. Parameters were learned from tests at C/3 in all cases.

Tests at C/2 and C were used to validate the model. A model disregarding self-discharge, cycle ageing and temperature effects was obtained.

The values of parameters τ , R_1 and R_2 are shown in Table 3 for the different batteries, as well as the measured average internal resistance, R_{int}, of the batteries [32], [40].

TABLE 2
CHARGING AND DISCHARGING CURRENTS DURING CYCLING

Battery	*Capacity (Ah)*	*I charge (A)*	*I charge cutoff (A)*	*I discharge C/3 – C/2 – C (A)*
MAN#1	100	30	5	33 – 50 - 100
MAN#2	100	30	5	33 – 50 - 100
MAN#3	16	4.8	0.8	5.33 – 8 - 16

In the model's present form, resistance R1 cannot be directly associated with the internal resistance, Rint, of the battery because the model was obtained using data sampled at 0.2 Hz from cycling tests, disregarding self-discharge, cycle ageing and temperature effects.

TABLE 3
PARAMETER VALUES OF THE TESTED BATTERIES

Battery	τ [s]	R_1 *[mΩ]*	R_2 *[kΩ]*	R_{int} *[mΩ]*
MAN#1	855	2.24	3.85	0.97
MAN#2	773	2.80	1.80	1.78
MAN#3	848	2.14	0.69	13.12

Considering the model as a complex impedance, at high frequencies, C_{eff} shortcuts R_2 and R_1 coincides with R_{int}. However, for small batteries with a low C_{eff}, the contribution of R_2 to R_{int} may still be significant at the Nyquist frequency and, thus R_1 in the model converges to a value lower than R_{int}.

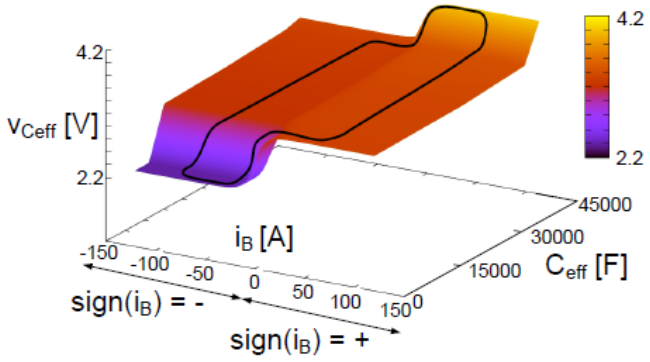

Fig. 7. Hysteresis cycle over the graph of $\rho(Q, sign(i_B))$, where $Q = C_{eff} \cdot v_{C_{eff}}$, for the MAN#2 battery. The function $\rho(Q, sign(i_B))$ has a similar shape for the other types of batteries.

Bearing this in mind, the values of R_{int} and R_1 were compared for the three types of batteries. The biggest difference is obtained for the 16 Ah battery. This is because the value of C_{eff} for the 100 Ah batteries is about 10 times higher than that for the 16 Ah battery. Thus, C_{eff} shortcuts R_2 at lower frequencies in the case of the 100 Ah batteries: that is the reason why R_1 is more similar to R_{int} in the case of these batteries.

The function $\rho(Q, sign(i_B))$, modeled by means of a FRBS, is shown for the MAN#2 battery. A cycle of hysteresis has been drawn over this graph; see Fig. 7. The voltage, $v_{C_{eff}}$, does not vary greatly for changes in charge, except when the battery is almost full or almost empty. As expected, the battery slope is high in these cases. The effective capacity, C_{eff}, ranges between 0 and 40000 F.

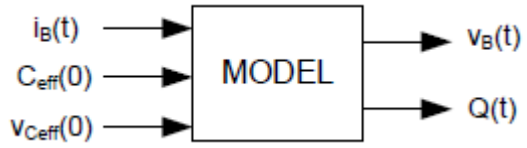

Fig. 8. Inputs and outputs of the battery model.

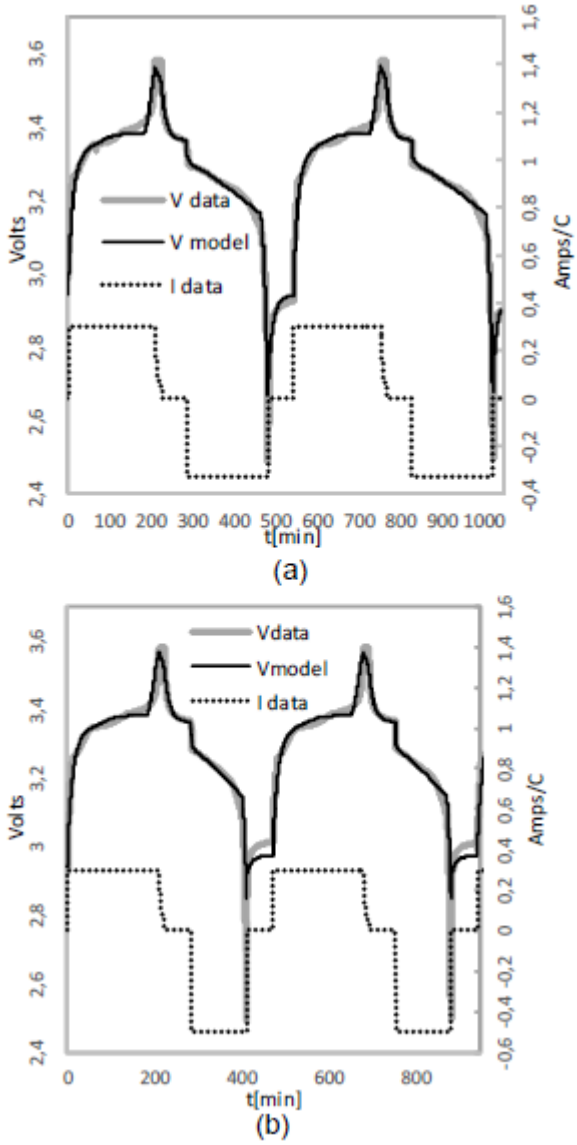

Fig. 9. Predicted and real voltages for the MAN#1 battery: a) Discharge at C/3. b) Discharge at C.

The model inputs are the initial stored electric charge, Q(0), which is given by $C_{eff}(0)$ and $v_{C_{eff}}(0)$, and the battery current, $i_B(t)$. The model outputs are the battery voltage, $v_B(t)$, and the stored electric charge, Q(t). See Fig. 8.

Fig. 9 shows real and predicted battery voltages for the MAN#1 battery at C and C/3 discharge rates. It can be seen that the predicted voltage reproduces the nonlinear behavior of the battery. The change in voltage slope at the end of the charge and discharge stages, the voltage hysteresis, the voltage changes during the rest periods and the voltage changes during the rest periods are all captured by the model.

The simulation in Fig. 9 starts at the beginning of a charge stage. The battery had been fully discharged previously, so Q(0)=0. The charge current in both cases is 30 A. Mean square errors of the predicted voltage were obtained for currents C/3, C/2 and C. Table 4 shows these errors for the different batteries.

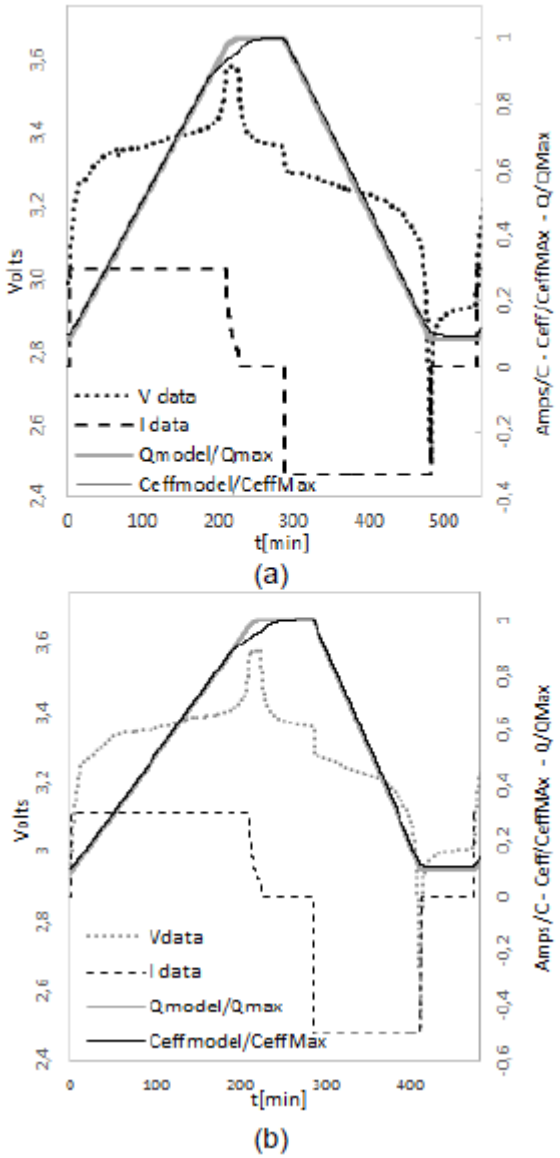

Fig. 10. Variation in stored charge and effective capacity during battery charge and discharge for the MAN#1 battery. a) Discharge at C/3. b) Discharge at C.

Fig. 10 shows the effective capacity of the battery and the stored charge during a charge/discharge cycle. It can be seen that the stored charge is considered constant during the inactivity period, though the effective capacity is not. This fact explains why the battery voltage changes during the periods of inactivity between the charge and discharge stages, which is the main contribution of the proposed model.

It should be noted that the voltage at the variable capacitor, $v_{C_{eff}}$, is not the OCV at equilibrium as in the case of the Thevenin- and impedance based- models. $v_{C_{eff}}$ is the OCV when no current flow through the battery, and $v_{C_{eff}}$ is only the OCV at equilibrium after a long rest period when the battery reaches equilibrium.

The product of the effective capacity multiplied by the capacitor voltage predicts the stored charge in the battery. The prediction of the stored charge in the MAN#1 battery is compared in Fig. 11 for three different discharge stages. The charge current in all cases is 30 A, although the discharge currents are respectively C/3, C/2 and C.

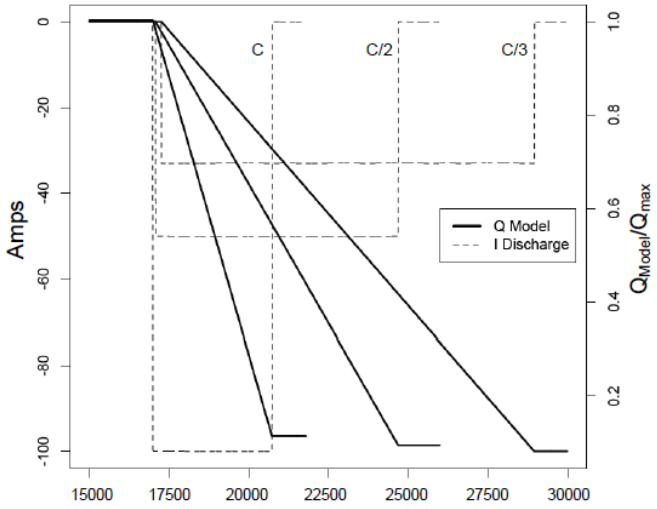

Fig. 11. Comparison of the extracted electric charge at C/3, C/2 and C discharges for the MAN#1 battery.

As the charge current is the same in all three cases, the amount of stored charge during the charge processes is also the same. However, the charge extracted from the battery differs depending on the discharge current. The smaller the discharge current, the longer the discharge process and hence the greater the extracted electric charge.

VII. Conclusions

A reliable equivalent circuit model that captures the nonlinear characteristics of battery behavior has been proposed. The equivalent effective capacity of the battery has been used to capture nonlinearities in the battery, instead of the OCV. The most important property of the proposed model versus other equivalent circuits is its capacity to reproduce the changes in battery voltage during resting periods, when no current flows through the battery.

Physical analogies have been used to explain how the proposed model works. A state-space nonlinear dynamic

model has been applied. A FRBS is embedded in the equations to model battery dynamics. Computational intelligence techniques are used to determine the unknown parameters of the model.

A model disregarding self-discharge, cycle aging and temperature effects has been validated using $LiFePO_4$ batteries. The agreement between simulations and experimental results shows that the proposed model accurately predicts battery voltage. The model is also able to predict the electrical charge stored in the battery.

Future developments will take into account the effect of temperature. Battery self-discharge and aging of the battery will also be incorporated in the model.

REFERENCES

[1] B. Scrosati and J. Garche, "Lithium batteries: Status, prospects and future," J. Power Sources, vol. 195, no. 9, pp. 2419-2430, May 2010.

[2] W.J. Zhang, "Structure and performance of LiFePO4 cathode materials: A review," J. Power Sources, vol. 196, no. 6, pp. 2962-2970, March 2011.

[3] A.A. Pesaran, "Choices and requirements of batteries for EVs, HEVs, PHEVs," National Renewable Energy Laboratory, NREL/PR-5400-51474, April 2011.

[4] G. L. Plett, "Extended Kalman filtering for battery management systems of LiPB-based HEV battery packs—Part 1. Background," J. Power Sources, vol. 134, no. 2, pp. 52–261, Aug. 2004.

[5] N.A. Chaturvedi, R. Klein, J. Christensen, J. Ahmed and A. Kojic, "Algorithms for Advanced Battery-Management Systems," IEEE Control Syst. Mag., vol. 30, no. 3, pp. 49-68, Jun. 2010.

[6] A. Szumanowski and Y. H. Chang, "Battery management system based on battery nonlinear dynamics modeling," IEEE Trans. Veh. Technol., vol. 57, no. 3, pp. 1425–1432, May 2008.

[7] A. Barre, B. Deguilhem, S. Grolleau, M. Gerard, F. Suard and D. Riu, "A review on lithium-ion battery ageing mechanisms and estimations for automotive applications," J. Power Sources, vol. 241, pp. 680–689, Nov. 2013.

[8] A. Barre, F. Suard, M. Gerard, M. Montaru and D. Riu, "Statistical analysis for understanding and predicting battery degradations in real-life electric vehicle use," J. Power Sources, vol. 245, pp. 846–856, Jan. 2014.

[9] J. Newman and W. Tiedemann, "Porous-Electrode Theory with Battery Applications," AIChe Journal, vol. 21, no. 1, pp. 25-41, Jan. 1975.

[10] K.E. Thomas, J. Newman and R. M. Darling, Advances in Lithium-ion Batteries, W. van Schalkwijk and B. Scrosati Eds. New York: Kluwer Academic/Plenum Publishers, 2002. pp. 345-392.

[11] M. Park el al., "A review of conduction phenomena in Li-ion batteries," J. Power Sources, vol. 195, no. 24, pp. 7904–7929, Dec. 2010.

[12] E. Martínez-Rosas, R. Vasquez-Medrano and A. Flores-Tlacuahuac, "Modeling and simulation of lithium-ion batteries," Computers and Chemical Engineering, vol. 29, no. 9, pp. 1937-1948, Sept. 2011.

[13] W. X. Shen, K. T. Chau, C. C. Chan, and E. W. C. Lo, "Neural network based residual capacity indicator for nickel-metal hydride batteries in electric vehicles," IEEE Trans. Veh. Technol., vol. 54, no. 5, pp. 1705–1712, Sep. 2005

[14] J. P. Wang, Q. S. Chen, and B. G. Cao, "Support vector machine based battery model for electric vehicles," Energy Convers. Manage. vol. 47, no. 7-8, pp. 858–864, May 2006.

[15] C. Bo, B. Zhifeng and C. Binggang, "State of charge estimation based on evolutionary neural network," Energy Convers. Manage. vol. 49, no. 10, pp. 2788-2794, Oct. 2008

[16] O. Linda et al, "Intelligent Neural Network Implementation for SOCI Development of Li-CFx Batteries," in Proc. IEEE IRCS 2009. pp. 57-62.

[17] M. Chen and G.A. Rincón-Mora. "Accurate electrical battery model capable of predicting runtime and I-V performance". IEEE Trans. Energy Convers., vol. 21, no. 2, pp. 504–511, June 2006.

[18] S. C. Hageman, "Simple pspice models let you simulate common battery types," EDN, pp. 17–132, Oct. 1993.

[19] S. Gold, "A Pspice macromodel for lithium-ion batteries," in Proc. 12th Annu. Battery Conf. Applications and Advances, 1997, pp. 215–222.

[20] A. Eddahech, O. Briat, N. Bertrand, J.-Y. Delétage and J.-M. Vinassa, "Behavior and state-of-health monitoring of Li-ion batteries using impedance spectroscopy and recurrent neural networks," Electrical Power & Energy Systems, vol. 42, no. 1, pp. 487-494, Nov 2012

[21] W. Wang, S. Käbitz and D.U. Sauer, "Experimental investigation of the lithium-ion battery impedance characteristic at various conditions and aging states and its influence on the application," Applied Energy, vol. 102, pp. 885-897, Feb. 2013.

[22] J. Xu, J.C. Mi, B. Cao and J. Cao, "A new method to estimate the state of charge of lithium-ion batteries based on the battery impedance model," J. Power Sources, vol. 233, pp 277-284, July 2013.

[23] M. A. Roscher and D. U. Sauer, "Dynamic electric behavior and open-circuit-voltage modeling of LiFePO4-based lithium ion secondary batteries," J. Power Sources, vol. 196, no. 1, pp. 331-336, Jan 2011.

[24] H. He, R. Xiong and H. Guo, "Online estimation of model parameters and state-of-charge of LiFePO4 batteries in electric vehicles," Applied Energy, vol. 89, no. 1, pp. 413-420, Jan 2012

[25] W.Y. Low, J.A. Aziz, N.R.N. Idris and R. Saidur, "Electrical model to predict current-voltage behaviours of lithium ferro phosphate batteries using a transient response correction method," J. Power Sources, vol. 221, pp. 201-209, Jan 2013. .

[26] J. Li, J.K. Barillas, C. Guenther and M.A. Danzer, "A comparative study of SOC estimation algorithms for LiFePO4 batteries used in electric vehicles," J. Power Sources, vol. 230, pp. 244-250. May 2013.

[27] L. Gao, S. Liu and R.A. Dougal, "Dynamic lithium-ion battery model for system simulations," IEEE Trans. Components and Packaging Tech., vol. 25, no. 3, pp. 495-505, Sept. 2002.

[28] S. Abu-Shark and D. Doerffel, "Rapid test and non-linear model characterization of solid-state lithium-ion batteries," J. Power Sources, vol. 130, no. 1-2, pp. 266-274, May 2004.

[29] R.C. Kroeze and P.T. Krein,"Electrical battery model for use in dynamic electric vehicle simulations," in Proc. IEEE PESC, Rhodes, Greece, 2008, pp. 1336-1342

[30] [30] T.A. Johansen and BA. Foss, "Identification of non-linear system structure and parameters using regime decomposition," Automatica, vol. 31, no. 2, pp. 321-326, Feb. 1995.

[31] O. Cordón, F. Herrera and F. Hoffman, "Genetic fuzzy systems: evolutionary tuning and learning of fuzzy knowledge bases," World Scientific, 2001.

[32] U.S.A.B.C Consortium (1996) Electric Vehicle Battery Test Procedure Manual. [Online]. Avalaible: http://www.uscar.org/guest/publications.php

[33] M. Dubarry, B.Y. Liaw.J, "Identify capacity fading mechanism in a commercial LiFePO4 cell," J. Power Sources, vol 194, no. 1, pp. 541-549, Oct. 2009

[34] L. Sánchez, I. Couso and M. González, "A design methodology for semi-physical fuzzy models applied to the dynamic characterization of LiFePO4 batteries," Applied Soft Computing, vol 14, part B, pp. 269-288, Jan. 2014.

[35] S.L. Chiu, "Fuzzy Model Identification Based on Cluster Estimation," J. Intelligent & Fuzzy Systems,v ol. 2, no. 3, pp. 267-279, Sept 1994.

[36] K. Loquing and O. Strauss, "Fuzzy Histograms and Density Estimation," In Soft Methods for Integrated Uncertainty Modelling. Germany. Springer Berlin Heidelberg 2006. pp. 45-52

[37] M. I. Jordan and D.E. Rumelhart, "Forward models: Supervised learning with a distal teacher," Cognitive Science, vol. 16, no. 3, pp. 307-354, Jul. 1992

[38] J.C. Butcher, The numerical analysis of ordinary differential equations: Runge-Kutta and general linear methods, New York. Wiley Interscience. New York. 1987.

[39] J.R. Villar and L. Sánchez, "Obtaining transparent models of chaotic systems with multiobjective simulated annealing algorithms," Information Sciences, vol. 178, no. 4, pp 952-970, Feb. 2008.

[40] B.V. Ratnakumar, M.C. Smart, L.D. Whitcanack and R.C. Ewell, "The impedance characteristics of Mars Exploration Rover Li-ion batteries," J. Power Sources, vol 159, no. 2, pp. 1428-1439, Sept. 2006.

Cecilio Blanco was awarded anMSc and PhD in Electrical Engineering from the University of Oviedo, Spain, in 1989 and 1996, respectively. In 1989, he joined the Department of Electrical and Electronic Engineering at the University of Oviedo, where he is currently Associate Professor and Head of the Instrumentation and Energy

Storage Systems Group. His research interests include electronic instrumentation systems and battery modeling.

Luciano Sánchez is a Full Professor at the Department of Computer Science, University of Oviedo. He is currently Head of the Metrology and Models Research Group and Founding Partner of the IDALIA S.L. spin-off from this research group. He has led four research projects funded by the Spanish government and 13 privately funded research contracts. He was an External Consultant with Electromateriales KLK from 1991–1995, Saint-gobain Cristaleria from 2000–2002, HC Energia from 2003–2005, IT- VASA from 2005–2008, and Indra Sistemas S.A. from 2010–2011. He enjoyed a stay as Visiting Scholar at the University of California at Berkeley in 1995 and at General Electric Global Research in 1996. His research interests include the theoretical study of algorithms for mathematical modeling and intelligent data analysis and the application of these techniques to practical problems of industrial modeling, signal processing, and dimensional metrology, with special interest in the study of low-quality data and fuzzy metainformation.
He is a member of the Editorial Board of three international journals, part of the steering committee of the Spanish *Metaheuristicas, Algoritmos Evolutivos y Bioinspirados* series of conferences, and of more than 60 Spanish and international conferences. He has co-authored more than 40 papers in international journal and more than 100 contributions to conferences and book chapters.

Manuela Gonzalez received an MSc and PhD in Electrical Engineering from the University of Oviedo, Spain, in 1992 and 1998, respectively. She is the founder and ead of the Battery Research Laboratory in the Department of Electrical and Electronic Engineering, at the University of Oviedo, where she holds the position of Associate Professor. Her research interests include battery management systems for new battery technologies and fast chargers for traction applications.

Juan C. Anton (M'08) was born in Veracruz, Mexico, in 1966. He was awarded an MSc in Computer Engineering from the University of Valladolid (Spain) in 1996. He received his PhD in 2007 from the University of Oviedo (Spain). He is currently an Associate Professor in the Department of Electrical and Electronic Engineering at the University of Oviedo. His research interests include lighting, electronic instrumentation systems and battery modeling.

Victor Garcia holds an MSc and PhD in Chemistry from the University of Oviedo. He is currently an Assistant Professor of Applied Electrochemistry in the area of Physical Chemistry. His research interests include fundamental aspects of applied electrochemistry. His recent work has focused on the electrical, chemical and thermal characterization of high power lithium ion cells with nanophosphate technology suitable for electric vehicles and he is involved in several research projects related to this technology.

Juan C. Viera was born in Havana, Cuba, in 1969. He received an MSc in Electrical Engineering from the University of Technology (ISPJAE), Havana, in 1992 and a PhD in Electrical Engineering from the University of Oviedo, Spain, in 2003. He held the position of Assistant Professor in the Department of Electrical Engineering at ISPJAE from 1992 to 1997. He currently holds the position of Assistant Professor in the Department of Electrical and Electronic Engineering, at the University of Oviedo, Spain. His research interests include battery testing, fast-charging and battery management systems.